JOURNAL OF GUIDANCE, CONTROL, AND DYNAMICS
Vol. 19, No. 3, May–June 1996

Variational Solutions for the Heat-Rate-Limited Aeroassisted Orbital Transfer Problem

Hans Seywald*
Analytical Mechanics Associates, Inc., Hampton, Virginia 23666

Minimum energy loss trajectories based on Pontryagin's minimum principle are generated for the atmospheric part of an aeroassisted orbital transfer problem. At the initial time all states are given. At the final time the altitude, velocity, and inclination change are prescribed. Additionally, the trajectory is subject to a heating rate limit, which, in the context of optimal control, represents a first-order state inequality constraint. Numerical difficulties implied by the singularly perturbed nature of the problem are avoided by starting the integration in the interior of the trajectory at a point where the heating rate limit is active. The state constraint becomes active always in the form of a state constrained arc. Nontrivial touch points have not been observed in numerical solutions.

I. Introduction

OVER the years a considerable amount of research has been conducted in the area of aeroassisted orbital transfers (AOT). Surveys on the current state of the art in optimization of AOT trajectories can be found in Refs. 1 and 2. The optimization of the atmospheric part of orbital plane changes using aerodynamic controls is discussed in Refs. 3–6. In Ref. 5, a guidance law is developed through regular expansion of the Hamilton–Jacobi–Bellmann equation. A guidance law development through matched asymptotic expansions and through a hybrid regular expansion/collocation approach is presented in Refs. 7 and 8, respectively. In Ref. 9, maximum cross range and maximum orbital plane change trajectories are calculated using a nonlinear programming code. In Ref. 10, the use of multiple pass trajectories is investigated to alleviate the severe aeroheating. In Ref. 11, aerocruise and aeroglide maneuvers are compared, both in presence of a heating rate limit.

Recently, variational solutions for the heating rate limited aerocruise maneuver were presented in Ref. 12. Numerical difficulties were reported, and converged solutions could not be obtained below a certain value for the prescribed maximum heating rate. The optimal switching structure was identified as (free, touch point, free). Solutions with state constrained arcs were not obtained. For the same vehicle model and atmospheric model as in Ref. 12 the heating rate limit could be reduced much further in Ref. 13, using direct shooting and direct collocation. The obtained trajectories are physically feasible and involve state constrained arcs. The solutions were reported to be very sensitive, and certain convergence difficulties were overcome by reducing the prescribed precision in the nonlinear program solver.

The present paper is based on a dynamical model that is identical to the one used in Ref. 12. The objective is to verify the results reported in Ref. 12, to identify the correct optimal switching structure, and to generate variational benchmark solutions that could be used to verify and to calibrate direct optimization approaches.

II. Problem Formulation

A. Optimal Control Problem

The problem considered in this paper is that of optimizing the atmospheric part of an aeroassisted orbital transfer. The control functions of time, aerodynamic lift C_L, and bank angle μ are to be determined such that a prescribed inclination change $\Delta i = 18$ deg is achieved with minimum energy loss and subject to a heating rate constraint. The states are radial distance r, geographic latitude ϕ, velocity v, flight path angle γ, and heading angle ψ. The following assumptions are made: point-mass model, Newtonian central gravitational field, air density varies exponentially with altitude, constant zero drag coefficient, and constant induced drag coefficient.

In dimensional form the problem is given as follows:

$$\min -v(t_f) \tag{1}$$

subject to the equations of motion

$$\begin{aligned} \dot{r} &= v\sin\gamma, \qquad \dot{\phi} = (v/r)\cos\gamma\sin\psi \\ \dot{v} &= -(D/m) - (\bar{\mu}/r^2)\sin\gamma \\ \dot{\gamma} &= \frac{L\cos\mu}{mv} + \left(\frac{v}{r} - \frac{\bar{\mu}}{r^2 v}\right)\cos\gamma \\ \dot{\psi} &= \frac{L\sin\mu}{mv\cos\gamma} - \frac{v}{r}\cos\gamma\cos\psi\tan\phi \end{aligned} \tag{2}$$

the control constraints

$$C_L \in [0, \infty) \tag{3}$$

$$\mu \in \boldsymbol{R} \tag{4}$$

the boundary conditions

$$r(0) = r_0 \tag{5a}$$

$$\phi(0) = 0 \tag{5b}$$

$$v(0) = v_0 \tag{5c}$$

$$\gamma(0) = \gamma_0 \tag{5d}$$

$$\psi(0) = 0 \tag{5e}$$

$$r(t_f) = r_0 \tag{5f}$$

$$\cos\phi(t_f)\cos\psi(t_f) = \cos(\Delta i) \tag{5g}$$

and a state inequality constraint of the general form

$$P_0(r, v) \le 0 \tag{6}$$

Specifically, P_0 is chosen such that condition (6) represents a heating rate limit $\dot{Q} \le \dot{Q}_{\max}$. The explicit functional forms of $\dot{Q}$ and P_0 are given in a later section in Eqs. (7) and (8). The numerical values of the gravitational constant $\bar{\mu}$, the quantities r_0, v_0, γ_0, and the prescribed inclination change Δi are given in Table 1.

B. Aerodynamic and Atmospheric Model

The aerodynamic drag and lift are given by

$$L = qAC_L, \qquad D = qAC_D$$

Received Aug. 29, 1994; revision received Oct. 15, 1995; accepted for publication Dec. 27, 1995.

*Supervising Engineer, working under contract at the Guidance and Controls Branch, NASA Langley Research Center. Member AIAA.

Table 1 Vehicle data, aerodynamic data, and physical constants

Quantity	Numerical value	Unit
r_e	20,926,430	ft
$\bar{\mu}$	1.408,95 10^{16}	ft^3/s^2
$r_0 - r_e$	365,000	ft
v_0	25,745.704	ft/s
γ_0	−0.55	deg
Δi	18	deg
A	125.84	ft^2
C_{D0}	0.032	1
K	1.4	1
ρ_s	$3.319{,}5 \times 10^{-5} \cdot e^{100{,}000[ft]/\beta}$	$slugs/ft^3$
g	$\bar{\mu}/r_e^2$	ft/s^2
v_s	$\sqrt{(\bar{\mu}/r_e)}$	ft/s
β	24,138.8	ft
m	331.5	slugs
$\bar{r}$	r_e	
$\bar{t}$	$\sqrt{(r_e^3/\bar{\mu})}$	
$\bar{m}$	m	

where C_L is the lift coefficient and

$$C_D = C_{D0} + KC_L^2$$

is the drag coefficient. The dynamic pressure q and the air density ρ are

$$q = \tfrac{1}{2}\rho v^2 \qquad \text{and} \qquad \rho = \rho_s e^{(r_e - r)/\beta}$$

respectively. The constants A, C_{D0}, K, ρ_s, r_e, and β denote reference area, zero drag coefficient, induced drag coefficient, air density at sea level, Earth's radius, and atmospheric scale height, respectively. The numerical values of all constants are given in Table 1.

C. Heating Rate Limit

As in Ref. 12, the heating rate $\dot{Q}$ in British thermal units per square foot per second is modeled through

$$\dot{Q} = 17{,}600\sqrt{(\rho/\rho_s)}(v/v_s)^{3.15} \tag{7}$$

Hence, with the functional dependence of P_0 on the radial distance r and the velocity v given by

$$P_0(r, v) = \sqrt{\frac{\rho}{\rho_s}}\left(\frac{v}{v_s}\right)^{3.15} - \frac{\dot{Q}_{\max}}{17{,}600} \tag{8}$$

condition (6) represents a heating rate limit $\dot{Q} \le \dot{Q}_{\max}$. Here, v_s denotes the circular orbit speed at the Earth's surface. The dimensional value of v_s as a function of $\bar{\mu}$ and r_e is given in Table 1.

D. Nondimensionalization

For numerical calculations the variables in the system description (2) are nondimensionalized with $\bar{r}$ = Earth's radius as the length scale, $\bar{m}$ = constant mass of the vehicle as the mass scale, and $\bar{t} = \sqrt{(r_e/g)}$ as the time scale. Here, $g = \bar{\mu}/r_e^2$ denotes the value of Earth's gravitational acceleration at radius r_e and $\bar{r}$, $\bar{m}$, and $\bar{t}$, are the usual canonical units used in astrodynamics.[14] Note that the unit speed $v_s = \bar{r}/\bar{t} = \sqrt{(\bar{\mu}/r_e)}$ corresponds to circular orbit speed at the Earth's surface. The quantities introduced in this section are summarized in Table 1.

III. Optimality Conditions

A. Nonconvexity of the Hodograph

An important issue in the theory of optimal control is the convexity of the hodograph. For fixed states x the hodograph $S(x)$ is defined as the set of all state rates $\dot{x}$ that can be achieved by varying the controls u within their admissible domains.[15] Nonconvexity of the hodograph may lead to analytical and numerical difficulties such as chattering control behavior and nonexistence of an optimal solution.

In the dynamical system (2) controls appear explicitly only in the right-hand sides of the $\dot{v}$, $\dot{\gamma}$, and $\dot{\psi}$ equations. In the associated subspace of the state rate space the hodograph is the two-dimensional surface manifold of a skewed paraboloid with its open end pointed in negative $\dot{v}$ direction. This hodograph is not convex.

In generating the numerical results presented in this paper the nonconvexity of the hodograph did not impose any difficulties. This, however, is only because of the benign multiplier directions observed in the obtained solutions, namely, $\lambda_v < 0$ generally, and $\lambda_\gamma^2 + \lambda_\psi^2 \neq 0$ along constrained arcs. If the boundary conditions are varied, these multiplier directions may change such that certain singular control cases become active. To perform the necessary analysis it is then required to modify the dynamical system (2) such that the hodograph associated with the new dynamical system becomes the convex hull of the original hodograph. Such analysis is not performed in the present paper.

B. Minimum Principle

Problems (1–6) and (8) are solved by applying the Pontryagin minimum principle.[16–18] Assuming that a solution of Eqs. (1–6) and (8) exists, the minimum principle states that at every point in time the control is such that the variational Hamiltonian

$$H = \lambda_r \dot{r} + \lambda_\phi \dot{\phi} + \lambda_v \dot{v} + \lambda_\gamma \dot{\gamma} + \lambda_\psi \dot{\psi} \tag{9}$$

is minimized subject to all control constraints

$$(\mu, C_L) = \arg \min_{(\mu, C_L) \in \Omega} H \tag{10}$$

$$\Omega = \left\{(\mu, C_L) \in \boldsymbol{R}^2 \middle| \mu, C_L \text{ are admissible}\right\} \tag{11}$$

On free arcs, i.e., on time intervals where Eq. (6) is satisfied with strict inequality,

$$\Omega = \left\{(\mu, C_L) \in \boldsymbol{R}^2 \middle| 0 \le C_L < \infty\right\} \tag{12}$$

On constrained arcs, i.e., on time intervals, say, $[t_1, t_2]$ where Eq. (6) is satisfied with strict equality,

$$P_0 \equiv 0 \qquad \text{on} \qquad [t_1, t_2] \tag{13}$$

is equivalent to

$$P_0 = 0 \qquad \text{at} \qquad t = t_1 \tag{14}$$

$$P_1 \equiv 0 \qquad \text{on} \qquad t \in (t_1, t_2) \tag{15}$$

where

$$P_1 := \frac{\mathrm{d}P_0}{\mathrm{d}t} = \frac{3.15}{v}\sqrt{\frac{\rho}{\rho_s}}\left(\frac{v}{v_s}\right)^{3.15}\left[-\frac{D}{m} - \left(\frac{\bar{\mu}}{r^2} + \frac{v^2}{6.3\beta}\right)\sin\gamma\right] \tag{16}$$

By noting that the terms in front of the square bracket in Eq. (16) are always positive, the condition $P_1 = 0$ can be replaced equivalently by

$$p_1 = 0 \tag{17}$$

where

$$p_1 = \left[-\frac{D}{m} - \left(\frac{\bar{\mu}}{r^2} + \frac{v^2}{6.3\beta}\right)\sin\gamma\right] \tag{18}$$

The set of admissible controls along state constrained arcs then takes the form

$$\Omega = \left\{(\mu, C_L) \in \boldsymbol{R}^2 \middle| 0 \le C_L < \infty,\ p_1 = 0\right\} \tag{19}$$

The evolution of the Lagrange multipliers λ_x, $x \in \{r, \phi, v, \gamma, \psi\}$ is governed by

$$\dot{\lambda}_x = -\frac{\partial H}{\partial x} \tag{20}$$

on unconstrained arcs. On constrained arcs, the implicit dependence of the controls on the states via the condition $p_1 = 0$ implies[19]

$$\dot{\lambda}_x = -\frac{\partial H}{\partial x} - \Lambda \frac{\partial p_1}{\partial x} \tag{21}$$

where Λ is the Kuhn–Tucker multiplier associated with the constraint (17) in the minimization problem Eqs. (10) and (19), i.e., Λ is determined from the condition

$$\frac{\partial H}{\partial C_L} + \Lambda \frac{\partial p_1}{\partial C_L} = 0 \tag{22}$$

Supplementary optimality conditions are given by[20,21]

$$\Lambda \geq 0 \tag{23}$$

$$\dot{\Lambda} \leq 0 \tag{24}$$

C. Hamiltonian and Adjoint Equations

Explicitly the Hamiltonian (9) takes the form

$$H = \lambda_r v \sin\gamma + \lambda_\phi \frac{v}{r}\cos\gamma \sin\psi - \lambda_v\left(\frac{D}{m} + \frac{\bar{\mu}}{r^2}\sin\gamma\right)$$
$$+ \lambda_\gamma\left[\frac{L\cos\mu}{mv} + \left(\frac{v}{r} - \frac{\bar{\mu}}{r^2 v}\right)\cos\gamma\right]$$
$$+ \lambda_\psi\left(\frac{L\sin\mu}{mv\cos\gamma} - \frac{v}{r}\cos\gamma\cos\psi\tan\phi\right) \tag{25}$$

and the adjoint equations can be stated as

$$\dot{\lambda}_r = -\frac{\partial H}{\partial r} - \Lambda\frac{\partial p_1}{\partial r}, \qquad \dot{\lambda}_\phi = -\frac{\partial H}{\partial \phi} - \Lambda\frac{\partial p_1}{\partial \phi}$$
$$\dot{\lambda}_v = -\frac{\partial H}{\partial v} - \Lambda\frac{\partial p_1}{\partial v}, \qquad \dot{\lambda}_\gamma = -\frac{\partial H}{\partial \gamma} - \Lambda\frac{\partial p_1}{\partial \gamma} \tag{26}$$
$$\dot{\lambda}_\psi = -\frac{\partial H}{\partial \psi} - \Lambda\frac{\partial p_1}{\partial \psi}$$

throughout the trajectory, where on free arcs

$$\Lambda = 0 \tag{27a}$$

and on constrained arcs

$$\Lambda = -\frac{\partial H}{\partial C_L}\left(\frac{\partial p_1}{\partial C_L}\right)^{-1} \tag{27b}$$

D. Control Logic

Along unconstrained arcs the minimum principle (10) with the admissible control set Ω given by Eq. (12) yields

$$\begin{bmatrix}\sin\mu\\ \cos\mu\end{bmatrix} = -\frac{1}{\sqrt{\lambda_\gamma^2 + (\lambda_\psi/\cos\gamma)^2}}\cdot\begin{bmatrix}\lambda_\psi/\cos\gamma\\ \lambda_\gamma\end{bmatrix} \tag{28}$$

and

$$C_L = -\frac{1}{2Kv\lambda_v}\cdot\sqrt{\lambda_\gamma^2 + (\lambda_\psi/\cos\gamma)^2} \tag{29}$$

Formally, we set

$$\Lambda = 0 \tag{30}$$

The expressions (28) and (29) are admissible only as along as $\lambda_v \neq 0$, and $\lambda_\gamma^2 + (\lambda_\psi/\cos\gamma)^2 \neq 0$. The classical Legendre–Clebsch condition $\partial^2 H/\partial C_L^2 \geq 0$ immediately implies $\lambda_v \leq 0$. Geometric arguments in the hodograph space yield the stronger condition $\lambda_v < 0$, as long as $\lambda_\gamma^2 + (\lambda_\psi/\cos\gamma)^2 \neq 0$. If $\lambda_\gamma^2 + (\lambda_\psi/\cos\gamma)^2 = 0$, then $\lambda_v = 0$ refers to a singular control case. Pointwise occurrence of this situation can be ignored. Assuming that $\lambda_\gamma^2 + (\lambda_\psi/\cos\gamma)^2 \equiv 0$ and $\lambda_v \equiv 0$ on some nonzero time interval requires (this can be shown through some simple calculations involving the conditions $\dot{\lambda}_v = 0$, $\dot{\lambda}_\gamma = 0$, $\dot{\lambda}_\psi = 0$, and $v \neq 0$, $\cos\gamma \neq 0$) that all multipliers $\lambda_r, \lambda_\phi, \lambda_v, \lambda_\gamma, \lambda_\psi$ are identically zero on this interval. Hence, the case $\lambda_v \equiv \lambda_\gamma^2 + (\lambda_\psi/\cos\gamma)^2 \equiv 0$ can be excluded. The case $\lambda_v \neq 0$, $\lambda_\gamma^2 + (\lambda_\psi/\cos\gamma)^2 = 0$ leads to an undefined expression in Eq. (28). This singularity, however, is only an artifact of the unfortunate parameterization of the admissible state rates in terms of the controls C_L and μ. Note that $\lambda_\gamma^2 + (\lambda_\psi/\cos\gamma)^2 = 0$ always implies $C_L = 0$ as long as $\lambda_v \neq 0$ [see Eq. (29)]. This, in return, removes all dependence of the right-hand side of the differential equations (2) on control μ. Hence, to overcome the singularity in Eq. (28) for $\lambda_\gamma^2 + (\lambda_\psi/\cos\gamma)^2 = 0$ it is clear that we can simply extend Eq. (28) by defining

$$\begin{bmatrix}\sin\mu\\ \cos\mu\end{bmatrix} = \begin{bmatrix}1\\ 0\end{bmatrix} \quad \text{if} \quad \lambda_\gamma^2 + (\lambda_\psi/\cos\gamma)^2 = 0 \tag{31}$$

Along constrained arcs the minimum principle (10) with the admissible control set Ω given by Eq. (19) yields

$$\begin{bmatrix}\sin\mu\\ \cos\mu\end{bmatrix} = -\frac{1}{\sqrt{\lambda_\gamma^2 + (\lambda_\psi/\cos\gamma)^2}}\cdot\begin{bmatrix}\lambda_\psi/\cos\gamma\\ \lambda_\gamma\end{bmatrix} \tag{32}$$

which is the same as in the unconstrained case. The control C_L and the multiplier Λ are given by

$$C_L = \sqrt{-\frac{C_{D0}}{K} - \frac{1}{qK}\left(\frac{1}{r^2} + \frac{\beta v^2}{6.3}\right)\sin\gamma} \tag{33}$$

and

$$\Lambda = -\lambda_v - \frac{\sqrt{\lambda_\gamma^2 + (\lambda_\psi/\cos\gamma)^2}}{2KvC_L} \tag{34}$$

respectively. In Eq. (34), C_L denotes the value of the lift coefficient obtained from Eq. (33).

For the constrained case, $\lambda_\gamma^2 + (\lambda_\psi/\cos\gamma)^2 = 0$ refers to a nontrivial singular case, which cannot be quickly discarded. Rigorous analysis of this singularity is possible only after convexizing the hodograph. As $\lambda_\gamma^2 + (\lambda_\psi/\cos\gamma)^2 \neq 0$ was obtained along all numerical solutions presented in this paper, such analysis is not given in the present paper.

E. Transversality and Corner Conditions

The transversality and corner conditions are given such that the first variation δJ of the cost function (1) $J = -v(t_f)$ is zero.[16,20] For the boundary conditions (5), this yields

$$\lambda_\phi(t_f) = -\nu\sin\phi(t_f)\cos\psi(t_f) \tag{35a}$$

$$\lambda_v(t_f) = -1 \tag{35b}$$

$$\lambda_\gamma(t_f) = 0 \tag{35c}$$

$$\lambda_\psi(t_f) = -\nu\cos\phi(t_f)\sin\psi(t_f) \tag{35d}$$

The free final time t_f is determined through the condition

$$H(t_f) = 0 \tag{36}$$

Because no explicitly time-dependent interior point constraints are imposed on the problem, the Hamiltonian H is continuous throughout the time interval $[0, t_f]$, including across corners.

At the beginning, say t_1, of the state constrained arc, conditions are

$$P_0|_{t_1} = 0 \tag{37a}$$

$$H|_{t_1^+} - H|_{t_1^-} = 0 \tag{37b}$$

$$\lambda_r(t_1^+) = \lambda_r(t_1^-) - l_0\left.\frac{\partial P_0}{\partial r}\right|_{t_1} \tag{37c}$$

$$\lambda_v(t_1^+) = \lambda_v(t_1^-) - l_0\left.\frac{\partial P_0}{\partial v}\right|_{t_1} \tag{37d}$$

where superscripts +, − denote evaluation at times $t_1 + \epsilon$, $t_1 - \epsilon$, $\epsilon > 0$, $\epsilon \to 0$, respectively. The jumps in the multipliers (37c) and (37d) involving the constant multiplier l_0 are implied by the interior point condition (37a). The end, say t_2, of the constrained arc is determined through

$$H|_{t_2^+} - H|_{t_2^-} = 0 \tag{38}$$

Here, in complete analogy to the nomenclature already used, the superscripts +, − denote evaluation at times $t_2 + \epsilon$, $t_2 - \epsilon$, $\epsilon > 0$, $\epsilon \to 0$, respectively.

IV. Numerical Implementation and Results

A. Some Analytically Equivalent Conditions

The conditions (37b) and (38) are usually not well suited for numerical implementation. In the following we state analytically equivalent expressions, which can be used to make numerical calculations more efficient or which can serve to check the obtained results.

First note that the functional dependence of $\sin\mu$ and $\cos\mu$ on states and costates is identical on free and constrained arcs [see Eqs. (28) and (32)]. Furthermore, all quantities appearing on the right-hand sides of Eqs. (28) and (32) are continuous across both switching points t_1 and t_2. This implies that $\sin\mu$ and $\cos\mu$ are continuous across t_1 and t_2, i.e.,

$$\begin{bmatrix} \sin\mu(t_1^+) \\ \cos\mu(t_1^+) \end{bmatrix} = \begin{bmatrix} \sin\mu(t_1^-) \\ \cos\mu(t_1^-) \end{bmatrix} \tag{39}$$

$$\begin{bmatrix} \sin\mu(t_2^+) \\ \cos\mu(t_2^+) \end{bmatrix} = \begin{bmatrix} \sin\mu(t_2^-) \\ \cos\mu(t_2^-) \end{bmatrix} \tag{40}$$

Now it can be verified that the condition (37b) is equivalent to the condition

$$C_L(t_1^+) = C_L(t_1^-) \tag{41}$$

To see this, we eliminate $\lambda_r(t_1^+)$, $\lambda_v(t_1^+)$ in Eq. (37b) through the jump conditions (37c) and (37d) and note that

$$\left.\frac{\partial P_0}{\partial x}\right|_{t_1} \dot{x}(t_1^+) = \left.\frac{\mathrm{d}P_0}{\mathrm{d}t}\right|_{t_1^+} = 0 \tag{42}$$

Then we obtain

$$\lambda(t_1^-)^T\left[\dot{x}(t_1^+) - \dot{x}(t_1^-)\right] = 0 \tag{43}$$

We used the notation $x = [r, \phi, v, \gamma, \psi]^T$, $\lambda = [\lambda_r, \lambda_\phi, \lambda_v, \lambda_\gamma, \lambda_\psi]^T$. The continuity of all states at t_1 and the condition (39) imply that all state rates, except possibly $\dot{v}$, are continuous across t_1, so that Eq. (43) reduces to

$$\lambda_v(t_1^-)^T\left[\dot{v}(t_1^+) - \dot{v}(t_1^-)\right] = 0 \tag{44}$$

As long as λ_v is guaranteed to be less than zero, this is equivalent to $\dot{v}(t_1^+) = \dot{v}(t_1^-)$ and, hence, to condition (41).

At t_2 the continuity of the Hamiltonian (38) is equivalent to either of the two conditions

$$C_L(t_2^+) = C_L(t_2^-) \tag{45}$$

$$\Lambda(t_2^-) = 0 \tag{46}$$

The equivalence of conditions (38) and (45) can be shown in complete analogy to the equivalence of conditions (37b) and (41), without the additional complication of jumps in the costates λ_r and λ_v. The equivalence of conditions (38) and (46) is established by inserting $C_L(t_2^+)$ obtained from Eq. (29) and $C_L(t_2^-)$ obtained from Eq. (34) into Eq. (45).

A useful expression for the height l_0 of the jump in the multipliers λ_r, λ_v in terms of states and costates evaluated at t_1^+ can be derived from Eq. (41). Explicitly, starting at Eq. (41) with $C_L(t_1^+)$ and $C_L(t_1^-)$ given by expressions (29) and (33), respectively, and eliminating $\lambda_v(t_1^-)$ in terms of $\lambda_v(t_1^+)$ through the jump condition (37d), yields after solving for l_0

$$l_0 = \left\{ -\lambda_v(t_1^+) - \frac{1}{2Kv} \times \sqrt{\frac{\lambda_\gamma^2 + (\lambda_\psi/\cos\gamma)^2}{-(C_{D0}/K) - [1/(qK)][(1/r^2) + (\beta/6.3)v^2]\sin\gamma}} \right\} \Bigg/ \left.\frac{\partial P_0}{\partial v}\right|_{t_1} \tag{47}$$

Upon backward integration of the trajectory across the switching point t_1, this expression can be used to eliminate the unknown parameter l_0 and to perform the costate jumps explicitly during the integration of the trajectory. Note that a similar expression for l_0 in terms of $\lambda_v(t_1^-)$ cannot be derived. Hence, explicit elimination of the jump multiplier l_0 is not possible upon forward integration of the trajectory.

B. Switching Structure

The switching structure is the temporal sequence in which different control logics become active along the optimal solution. Generally, the switching structure is not known in advance and has to be determined through smart guessing and numerical experiments.

For the present problem a direct optimization method[22] was utilized to generate approximate solutions. With respect to the state

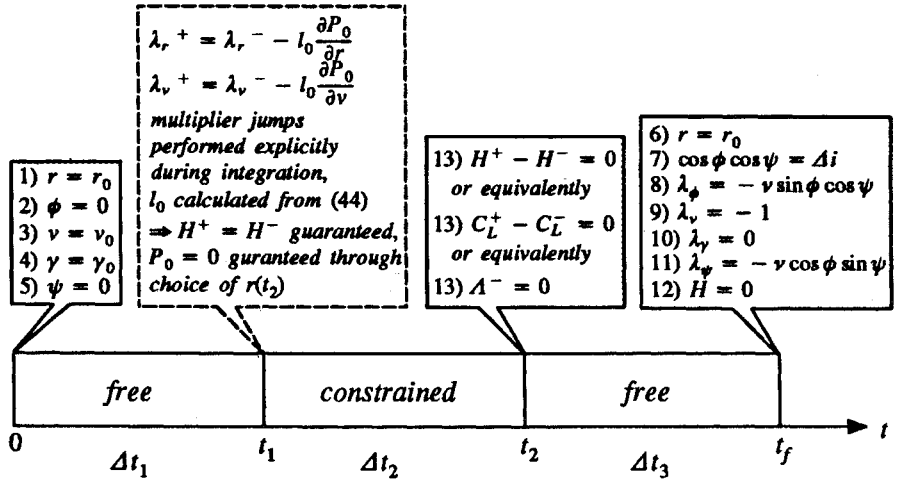

Fig. 1 Schematic representation of the boundary value problem associated with the switching structure free–constrained–free. Thirteen parameters: $\phi(t_2)$, $v(t_2)$, $\gamma(t_2)$, $\psi(t_2)$, $\lambda_r(t_2)$, $\lambda_\phi(t_2)$, $\lambda_v(t_2)$, $\lambda_\gamma(t_2)$, $\lambda_\psi(t_2)$, Δt_1, Δt_2, Δt_3, ν; 13 conditions: see above.

constraint (6), this approach predicted the switching structure (free, constrained, free). The direct optimization approach also predicted the absence of singular control arcs. This reduced the analytical and numerical work load considerably.

The limited resolution of direct optimization approaches makes it impossible, at times, to distinguish clearly between constrained arcs and touch points, especially when the constrained arcs are of very short duration, as in the present problem. It is known that for first-order state inequality constraints touch points can occur only in certain special cases.[20,23,24] Applying Corollary 10 of Ref. 24 to the present problem, it can be shown that a nontrivial touch point t_1 requires $C_L(t_1) = 0$. This condition is violated in the numerical solutions obtained through direct optimization. Thus, a clear indication is obtained that there is no touch point except in the

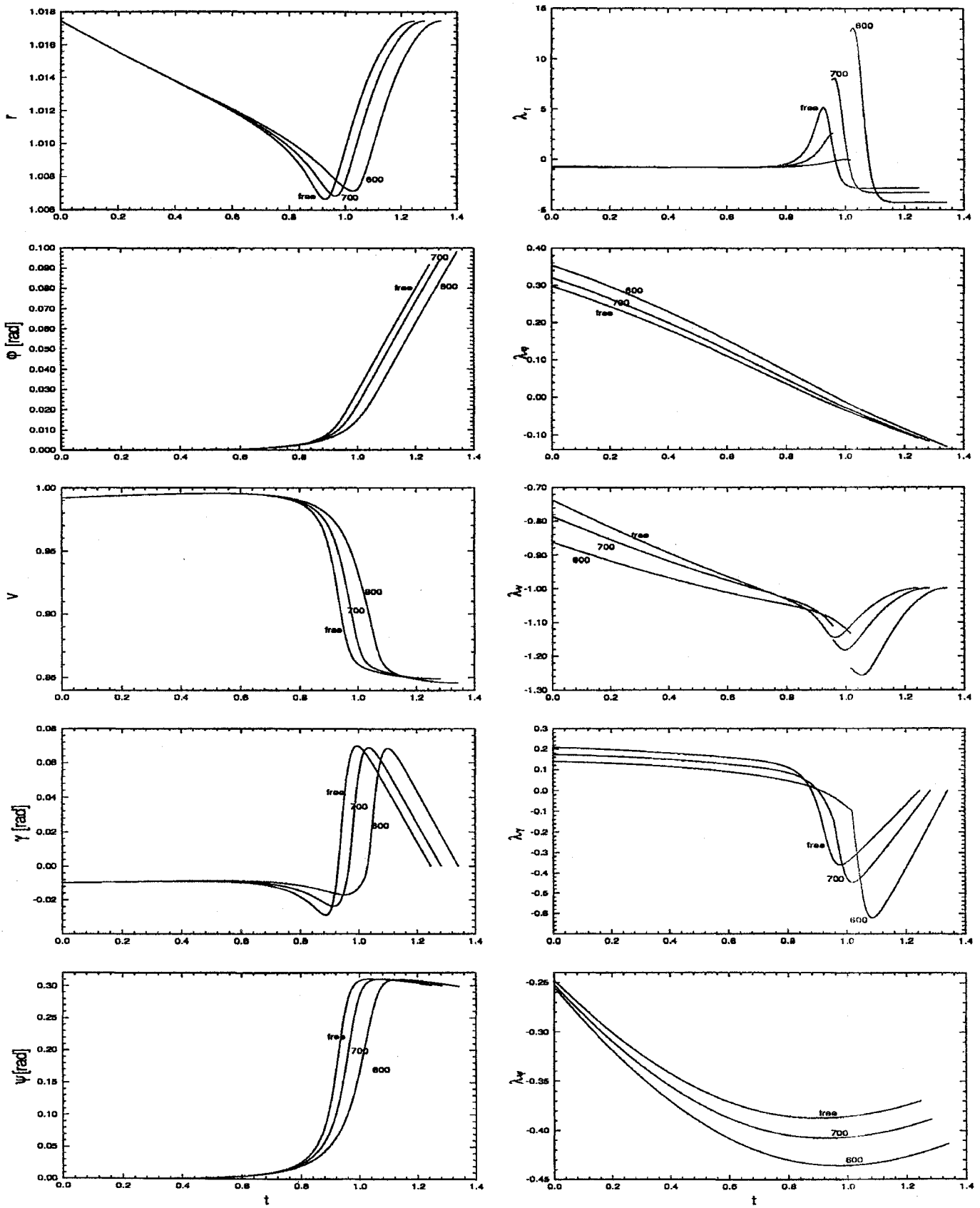

Fig. 2 States and costates vs time t for $\dot{Q}_{max}$ = 600, 700, and free.

trivial case where the unconstrained solution marginally touches the constraint.

In summary, based on numerical results obtained from a direct optimization approach and based on analytical results obtained in Ref. 24, the optimal switching structure was guessed to be of the form (free, constrained, free). Numerical results obtained with a high-precision indirect method confirm this guess as being correct, as shown in a later section.

C. Boundary Value Problem

The structure of the boundary value problem implied by the optimality conditions stated in the preceding sections clearly depends on the switching structure. In the following, we always assume the switching structure to be (free, constrained, free), which is optimal for all numerical solutions presented in this paper. The evolution of the states and costates is then described by the state equations (2), the costate equations (26), and the jump conditions (37c) and (37d). The controls C_L and η and the multiplier Λ are given by Eqs. (28–30) along the unconstrained arcs and by Eqs. (32–34) along the constrained arc. The boundary value problem can then be cast as the problem of finding the 17 scalar unknowns $r(0)$, $\phi(0)$, $v(0)$, $\gamma(0)$, $\psi(0)$, $\lambda_r(0)$, $\lambda_\phi(0)$, $\lambda_v(0)$, $\lambda_\gamma(0)$, $\lambda_\psi(0)$, $\lambda_r(t_2^+)$, $\lambda_v(t_2^+)$, Δt_1, Δt_2, Δt_3, l_0, and ν such that the 17 scalar constraints given by Eqs. (5) and (35–38) are satisfied. Here, the nonnegative quantities Δt_1, Δt_2, and Δt_3 denote the lengths of the three subarcs of the trajectory, respectively. It is clear that several parameters can be eliminated analytically, e.g., the parameters $r(0)$, $\phi(0)$, $v(0)$, $\gamma(0)$, and $\psi(0)$ can be determined explicitly through the conditions (5a–5e), and, if backward integration is chosen in favor over forward integration, the parameters l_0, $\lambda_r(t_2^+)$, and $\lambda_v(t_2^+)$ can be deleted by performing the multiplier jumps (37c) and (37d) explicitly during the integration of the trajectory, as discussed in an earlier section.

With or without these simplifications, however, the boundary value problem as cast is numerically not well behaved. Because of the exponentially increasing air density at lower altitudes the state rates increase dramatically near $h = h_{\min}$ (h denotes altitude and $h_{\min}$ denotes the lowest altitude reached along a trajectory). The singularly perturbed nature of the dynamical system has the effect that small changes in states/costates at initial time may have large effects on states/costates near $h_{\min}$. These perturbations become a numerical problem if at some stage during the iterative process of solving the boundary value problem the value of the state constraint P_0 becomes significantly nonzero at the beginning of the constrained arc. Note that, upon forward integration of the trajectory, the beginning of the state constrained arc, t_1, is determined by the length Δt_1 of the first unconstrained arc, not by the condition $P_0|_{t_1} = 0$ [P_0 as in Eq. (8)]. The latter condition is guaranteed to be satisfied only for the converged solution. Because the control C_L in Eq. (33) is determined such that $dP_0/dt = 0$ along the constrained arc, even a small increase in $P_0|_{t_1}$ can cause the vehicle to run out of energy along the constrained arc. This typically leads to a negative square root in Eq. (33) and the iteration breaks down.

D. Alternative Boundary Value Problem

To overcome the difficulties mentioned in the preceding section, the intregation of the trajectory is started at the end of the constrained arc, t_2. Formally, the states and costates at time t_2 then play the role of unknown initial states. By deleting $r(t_2)$ from this set of unknowns, and by calculating $r(t_2)$ explicitly from the condition $P_0|_{t_1} = 0$ [P_0 as in Eq. (8)], it is guaranteed that the state constraint (13) is correctly satisfied throughout the constrained arc at any stage during the iteration, even before convergence is achieved. Explicitly, the boundary value problem then reduces to finding the 16 parameters $\phi(t_2)$, $v(t_2)$, $\gamma(t_2)$, $\psi(t_2)$, $\lambda_r(t_2)$, $\lambda_\phi(t_2)$, $\lambda_v(t_2)$, $\lambda_\gamma(t_2)$, $\lambda_\psi(t_2)$, $\lambda_r(t_1^-)$, $\lambda_v(t_1^-)$, Δt_1, Δt_2, Δt_3, l_0, and ν such that the 16 conditions (5a–5g), (35a–35d), (36), (37b–37d), and (38) are satisfied. By making use of Eq. (47) and by performing the jump in the multipliers λ_r and λ_v explicitly during the integration, the parameters l_0, $\lambda_r(t_1^-)$, and $\lambda_v(t_1^-)$ can be deleted from the list of unknowns and the associated equations (37b–37d), can be deleted from the set of conditions. A schematic representation of this boundary value problem is given in Fig. 1.

E. Numerical Results

For a numerical treatment of the problem, the heating rate constraint $\dot{Q}_{\max}$ is varied between 600 and 771.676 BTU/ft^{2}s, the latter being the maximum attained value of $\dot{Q}$ if the heating rate limit is deleted. For all solutions the switching structure remains the same, namely, (free, constrained, free). For the case $\dot{Q}_{\max} = 600$ BTU/ft^{2}s, the length of the constrained arc is 0.00154 nondimensional time units (=1.242 s) and reduces monotonically when $\dot{Q}_{\max}$ is increased. At $\dot{Q}_{\max} = 771.676$ BTU/ft^{2}s, the constrained arc has degenerated to a single point, so that the switching times t_1 and t_2 coincide and represent a trivial touch point. Clearly, the solution remains unaffected if $\dot{Q}_{\max}$ is increased further to values greater than 771.676 BTU/ft^{2}s. The time histories of the states, costates, controls, and the heating rate $\dot{Q}$ for several different prescribed values of the heating rate constraint $\dot{Q}_{\max}$ are shown in Figs. 2–5. The lengths of the state constrained arc, the optimal final times, and the optimal final velocities for these trajectories are summarized in Table 2.

Further numerical results show that the switching structure (free, constrained, free) becomes inactive for heating rate limits $\dot{Q}_{\max}$ significantly lower than 600 BTU/ft^{2}s. (For $\dot{Q}_{\max} = 455$ BTU/ft^2 s, this switching structure is still optimal; for $\dot{Q}_{\max} \leq 450$ BTU/ft^{2}s, it is incorrect.) Numerical solutions to the first-order necessary conditions can still be obtained under the assumption that the switching structure is (free, constrained, free). However, the so-obtained

Table 2 Some characteric results as a function of the maximum heating rate limit

$\dot{Q}_{\max}$	Δt_2, s	t_f, s	$v(t_f)$, m/s
771.676 (free)	0.000	1005.877	6718.864
700	0.292	1034.706	6714.103
600	1.243	1082.117	6688.533

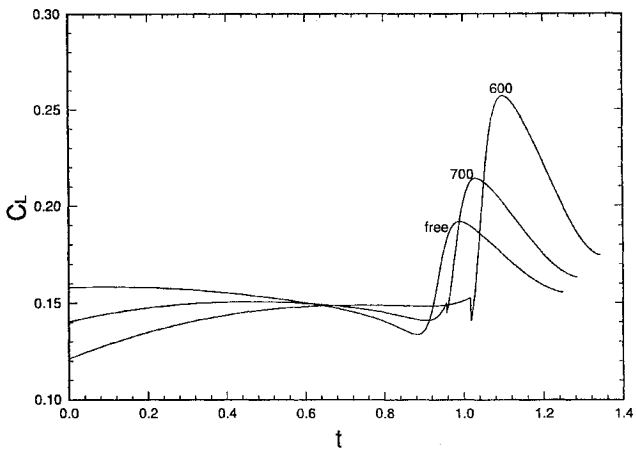

Fig. 3 Lift coefficient C_L vs time t for $\dot{Q}_{\max}$ = 600, 700, and free.

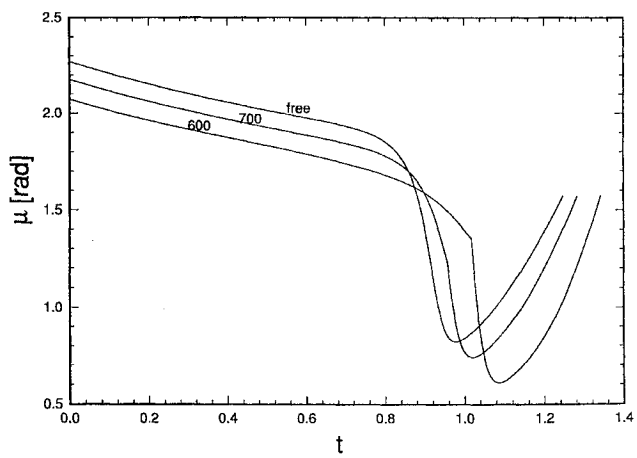

Fig. 4 Bank angle μ vs time t for $\dot{Q}_{\max}$ = 600, 700, and free.

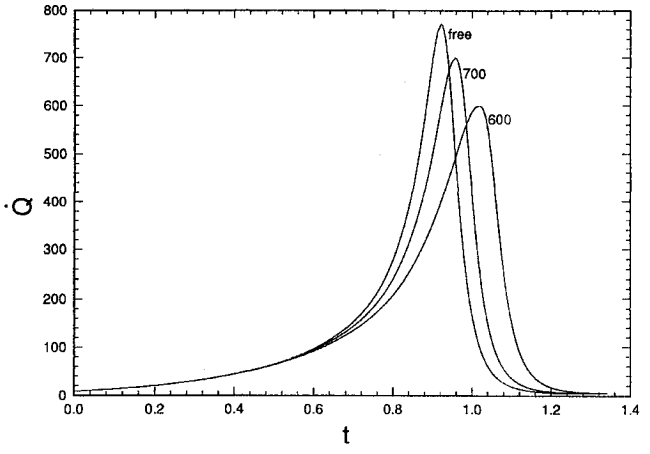

Fig. 5 Heating rate $\dot{Q}$ vs time t for $\dot{Q}_{max}$ = 600, 700, and free.

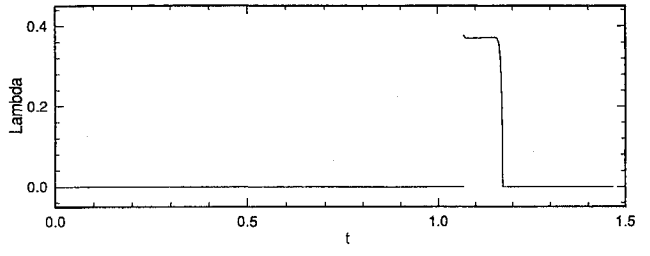

Fig. 6 Multiplier Λ vs time t for Q_{max} = 400.

solutions violate the condition (24) along the constrained arc, which is demonstrated in Fig. 6 for the example $\dot{Q}_{max} = 400$ BTU/ft^{2}s. Note that the associated solution is, in fact, a physically flyable trajectory, in the sense that all physical constraints (2–6) are satisfied. Only the cost index (1) is no longer optimal. Attempts to identify the switching structure using direct methods were unsuccessful. Several numerical experiments were attempted to generate a numerical solution with the switching structure (free, constrained, free, constrained, free), but convergence could not be achieved. A hypothesis is that the optimal solutions for $\dot{Q}_{max} \leq 450$ BTU/ft^{2}s involve at least three constrained arcs.

V. Summary and Conclusions

Variational solutions for the atmospheric part of an aeroassisted orbital transfer subject to a heating rate limit are presented. The optimal switching structure is found to consist of three arcs, namely, two unconstrained arcs and, in between, one arc along which the heating rate limit is satisfied with strict equality. In all solutions the state constrained arc is very short compared to the free arcs. Touch points have not been encountered, however, except in the trivial case where the unconstrained solution satisfies the heating rate limit marginally at a single point. This result contradicts results published previously.

Numerical solutions are generated with simple shooting. The inherent ill conditioning of the problem resulting from the exponential atmospheric model is overcome by starting the integration at a conveniently chosen point in the interior of the trajectory. Numerical solutions are presented for several different values of the heating rate limit.

Acknowledgment

This work was supported by NASA Langley Research Center under Contract NAS1-18935.

References

[1]Walberg, G. D., "A Survey of Aeroassisted Orbital Transfer," *Journal of Spacecraft and Rockets*, Vol. 22, No. 1, 1985, pp. 3–18.

[2]Mease, K. D., "Optimization of Aeroassisted Orbital Transfer: Current Status," *Journal of the Astronautical Sciences*, Vol. 36, Nos. 1/2, 1988, pp. 7–33.

[3]Vinh, N. X., and Hanson, J. M., "Optimal Aeroassisted Return from High Earth Orbit with Plane Change," *Acta Astronautica*, Vol. 12, No. 1, 1985, pp. 11–15.

[4]Hull, D. G., Giltner, J. L., Speyer, J. L., and Mapar, J., "Minimum Energy-Loss Guidance, for Aeroassisted Orbital Plane Change," *Journal of Guidance, Control, and Dynamics*, Vol. 8, No. 4, 1985, pp. 487–493.

[5]Speyer, J. L., and Crues, Z., "Approximate Optimal Atmospheric Guidance Law for Aeroassisted Plane-Change Maneuvers," *Journal of Guidance, Control, and Dynamics*, Vol. 13, No. 5, 1990, pp. 792–802.

[6]Calise, A. J., and Bae, G., "Optimal Heading Change with Energy Loss for a Hypersonic Gliding Vehicle," *Journal of Guidance, Control, and Dynamics*, Vol. 13, No. 4, 1990, pp. 609–614.

[7]Melamed, N., "Guidance Law Development for Aeroassisted Transfer Vehicles Using Matched Asymptotic Expansions," Ph.D. Thesis, School of Aerospace Engineering, Georgia Inst. of Technology, Atlanta, GA, Sept. 1993.

[8]McFarland, M. B., and Calise, A. J., "A Hybrid Approach to Near-Optimal Atmospheric Guidance for Aeroassisted Orbit Transfer Maneuvers," AIAA Paper 93-3858, July 1993.

[9]Hull, D. G., and Speyer, J. L., "Optimal Reentry and Plane Change Trajectories," *Journal of the Astronautical Sciences*, Vol. 30, No. 2, 1982, pp. 117–130.

[10]Rehder, J. J., "Multiple Pass Trajectories for an Aeroassisted Orbital Transfer Vehicle," AIAA Paper 84-0407, Jan. 1984.

[11]Lee, J. Y., and Hull, D. G., "Maximum Orbit Plane Change with Heat-Transfer-Rate Considerations," *Journal of Guidance, Control, and Dynamics*, Vol. 13, No. 3, 1989, pp. 492–497.

[12]Bae, G., and Calise, A. J., "Optimal Aeroglide and Orbit Plane Change of an Aeroassisted Orbit Plane Change Vehicle with an Aerodynamic Heating Rate Constraint," AIAA Paper 93-3678, Aug. 1993.

[13]Zimmermann, F., and Calise, A. J., "Aeroassisted Orbital Transfer Trajectory Optimization Using Direct Methods," AIAA Paper 95-3478, Aug. 1995.

[14]Bate, R. R., Mueller, D. D., and White, J. E., *Fundamentals of Astrodynamics*, Dover, New York, 1971.

[15]Cliff, E. M., Seywald, H., and Bless, R. R., "Hodograph Analysis in Aircraft Trajectory Optimization," AIAA Paper 93-3742, Aug. 1993.

[16]Bryson, A. E., and Ho, Y. C., *Applied Optimal Control*, Hemisphere, New York, 1975.

[17]Lee, E. B., and Markus, L., *Foundations of Optimal Control Theory*, Krieger, Malabar, FL, 1986.

[18]Neustadt, L. W., *A Theory of Necessary Conditions*, Princeton Univ. Press, Princeton, NJ, 1976.

[19]Bryson, A. E., Denham, W. F., and Dreyfus, S. E., "Optimal Programming Problems with Inequality Constraints, I: Necessary Conditions for Extremal Solutions," *AIAA Journal*, Vol. 1, No. 11, 1963, pp. 2544–2550.

[20]Jacobson, D. H., Lele, M. M., and Speyer, J. L., "New Necessary Conditions of Optimality for Control Problems with State-Variable Inequality Constraints," *Journal of Mathematical Analysis and Application*, Vol. 35, No. 2, 1971, pp. 255–284.

[21]Kreindler, E., "Additional Necessary Conditions for Optimal Control with State-Variable Inequality Constraints," *Journal of Mathematical Analysis and Application*, Vol. 35, No. 2, 1971, pp. 255–284.

[22]Seywald, H., "Trajectory Optimization Based on Differential Inclusion," *Journal of Guidance, Control, and Dynamics*, Vol. 17, No. 3, 1994, pp. 480–487.

[23]Maurer, H., and Gillessen, W., "Application of Multiple Shooting to the Numerical Solution of Optimal Control Problems with Bounded State Variables," *Computing*, Vol. 15, Fasc. 2, 1975, pp. 105–126.

[24]Seywald, H., and Cliff, E. M., "On the Existence of Touch Points for First-Order State Inequality Constraints," *Proceedings of the AIAA Guidance, Navigation, and Control Conference* (Monterey, CA), AIAA, Washington, DC, 1993, pp. 372–376.